Kinetic Monte Carlo modeling of the efficiency roll-off in a multilayer white OLED

M. Mesta,[1] H. van Eersel,[2] R. Coehoorn,[1] and P.A. Bobbert[1]
[1)] *Department of Applied Physics, Technische Universiteit Eindhoven, P.O. Box 513, NL-5600 MB Eindhoven, The Netherlands*
[2)] *Simbeyond B.V., P.O. Box 513, NL-5600 MB Eindhoven, The Netherlands*

(Dated: March 11, 2016)

Triplet-triplet annihilation (TTA) and triplet-polaron quenching (TPQ) in OLEDs lead to a roll-off of the internal quantum efficiency (IQE) with increasing current density J. We employ a kinetic Monte Carlo modeling study to analyze the measured IQE and color balance as function of J in a multilayer hybrid white OLED that combines fluorescent blue with phosphorescent green and red emission. We investigate two models for TTA and TPQ involving the phosphorescent green and red emitters: short-range nearest-neighbor quenching and long-range Förster-type quenching. Short-range quenching predicts roll-off to occur at much higher J than measured. Taking long-range quenching with Förster radii for TTA and TPQ equal to twice the Förster radii for exciton transfer leads to a fair description of the measured IQE-J curve, with the major contribution to the roll-off coming from TPQ. The measured decrease of the ratio of phosphorescent to fluorescent component of the emitted light with increasing J is correctly predicted. A proper description of the J-dependence of the ratio of red and green phosphorescent emission needs further model refinements.

The introduction of phosphorescent emitters in white organic light-emitting devices (OLEDs) has gained much interest due to the possibility of obtaining a very high internal quantum efficiency (IQE).[1–3] The strong spin-orbit coupling of the heavy metal atoms in phosphorescent emitters allows not only singlet, but also triplet excitons to decay radiatively. However, the triplet excitons still have a much longer lifetime than the singlet excitons, so that they are more vulnerable to quenching. Triplet-triplet annihilation (TTA) and triplet-polaron quenching (TPQ) have been identified as important quenching mechanisms.[4–6] Exciton quenching will increase in importance when the current density and brightness level of the OLED increase, since the densities of charge carriers and excitons are then higher. The drop in efficiency with increasing current density as a result of exciton quenching is known as the efficiency roll-off. A better understanding of the factors that determine this roll-off is crucial, because in practice one would like to use OLEDs for lighting and displays at the highest possible brightness level. Moreover, exciton quenching may also be a source of material degradation, because the involved high excitation energies may lead to breaking of chemical bonds and hence to a loss of functionality of the used materials.[7,8]

In previous work,[9] we studied by kinetic Monte Carlo (kMC) simulations the electronic processes that lead to electroluminescence in a hybrid multilayer white OLED, of which the stack structure and energy levels are given in Figure 1. The hybrid character of this OLED lies in the combined use of a fluorescent blue emitter (Spiro-DPVBi) with a phosphorescent green ($Ir(ppy)_3$) and red ($Ir(MDQ)_2(acac)$) emitter. Hybrid OLEDs are commercially important, despite the suboptimal efficiency due to the use of a blue fluorescent emitter, since as yet no sufficiently stable blue phosphorescent emitter for OLEDs exists. In this OLED an important role is played by the interlayer in between the blue and green emitting layers.

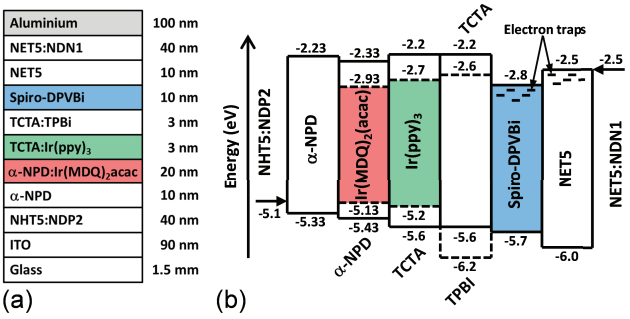

Figure 1. (a) Layer structure of the studied OLED (surface area: 2.7× 2.5 mm). From bottom to top: glass, indium tin oxide, p-doped hole-injecting layer of NHT5 with 4 mol% NDP2 (materials supplied by Novaled), hole-transporting layer of α-NPD, red-emitting layer of α-NPD with 5 mol% $Ir(MDQ)_2(acac)$, green-emitting layer of TCTA with 8 mol% $Ir(ppy)_3$, interlayer of the hole transporter TCTA with 33 mol% of the electron transporter TPBi, blue-emitting layer of Spiro-DPVBi, electron-transporting layer of NET5, and n-doped electron-injecting layer of NET5 with 4 mol% NDN1 (materials supplied by Novaled). (b) Corresponding energy levels. The arrows indicate the work functions used for the doped hole- and electron-injecting layers. See Ref. 9 for further details.

This interlayer, consisting of a mixture of an electron (TPBi) and hole (TCTA) transporter, should allow passage of electrons and holes in opposite directions, while blocking triplet excitons from transferring from the green emitter to the energetically lower-lying triplet level in the blue fluorescent layer.

In Ref. 9, a two-step procedure was followed in the simulations by first simulating the charge dynamics, including exciton formation, and subsequently the exciton dynamics. The resulting simulated emission profile and color balance were found to agree well with experiment, but exciton quenching could not be investigated because

of the decoupling of charge and exciton dynamics. In this Letter we consider exactly the same OLED of Figure 1, but treat charge and exciton dynamics together with exciton quenching in a fully integrated way. We recently performed such integrated simulations for monochrome OLEDs.[8,10] In this Letter, such simulations are applied to a realistic multilayer white OLED.

The details of the kMC simulation procedure were given in Ref. 9. We repeat here only the most important aspects. The molecular sites in the organic layers are modeled as a simple cubic lattice with a lattice constant of 1 nm, corresponding to the typical intermolecular distance. Energies of the highest (lowest) occupied (unoccupied) molecular orbitals, HOMO (LUMO), are assigned to the sites according to Figure 1, with the addition of a random energy of a correlated disorder model with a standard deviation $\sigma = 0.1$ eV. Emitter sites in the green and red layer are randomly assigned according to their known concentrations. Electron trap sites in the electron transporting layer (NET5) and the blue emitting layer are randomly assigned and given an energy drawn from an exponential distribution, according to model studies of electron transport in these layers. The electron- and hole-injecting n- and p-doped layers are modeled as sheets of metallic-like sites with energies indicated by arrows in Figure 1. These sites can inject or collect an arbitrary number of charges. Coulomb interactions and image charge effects are included. Site-to-site hopping of charges occurs by a Miller-Abrahams hopping rate, with a prefactor chosen such that measured or assumed electron and hole mobilities of the different materials in the stack at room temperature, low electric field, and low carrier concentration, are reproduced. The use of Marcus hopping rates would be more appropriate, but introduces as new parameters the reorganization energies of all the materials in the stack. For a low electric field the difference in mobility functions following from Miller-Abrahams and Marcus hopping rates was shown to be small.[11]

In Ref. 9, exciton formation was assumed to be always an irreversible energetically downward process. Here, we take into account the finite exciton lifetime, its binding energy, and the possibility of its dissociation and quenching. An exciton is modeled as an electron-hole pair at a site with an energy equal to the HOMO-LUMO energy difference with the exciton binding energy subtracted. Charge carriers generated from dissociated excitons can again participate in exciton formation. In the blue fluorescent layer we take an exciton binding energy of 0.5 eV, whereas in the interlayer and in the green and red phosphorescent layers we take a triplet exciton binding energy of 1.0 eV, which is a typical value.[12]

Like in Ref. 9, we assume that 25% of the excitons formed in the blue fluorescent layer are singlets and that the 75% formed triplets are lost. In the green- and red-emitting layers, excitons are either formed directly on the emitters, or on the host molecules (TCTA and α-NPD, respectively), followed by immediate transfer to an emitter in their neighborhood. Excitons formed in the interlayer (a significant fraction) and in all other layers (a negligible fraction) are assumed to be lost.

The mixing in of singlet character by the iridium spin-orbit coupling allows for radiative decay of the triplet excitons as well as their Förster transfer in between the phosphorescent emitters, including transfer from green to red emitters. The transfer rate between two emitters i and j is[13]

$$r_{\mathrm{F},ij} = \frac{1}{\tau_i}\left(\frac{R_{\mathrm{F},ij}}{R_{ij}}\right)^6, \qquad (1)$$

where τ_i is the radiative decay lifetime of emitter i, R_{ij} the distance between the two emitters, and $R_{\mathrm{F},ij}$ the Förster radius for transfer from i to j. The Förster radius depends on the spectral overlap between the emission spectrum of i and the absorption spectrum of j. Excitons can decay radiatively with a rate $\Gamma_{\mathrm{r},i} = 1/\tau_{\mathrm{r},i}$, or non-radiatively with a rate $\Gamma_{\mathrm{nr},i} = 1/\tau_{\mathrm{nr},i}$. These rates are related to the radiative decay probabilities $\eta_{\mathrm{r},i}$ by $\eta_{\mathrm{r},i} = \Gamma_{\mathrm{r},i}/(\Gamma_{\mathrm{r},i} + \Gamma_{\mathrm{nr},i})$. The parameters used in the exciton dynamics are taken from literature. For the singlets formed in the blue fluorescent layer we take $\eta_{\mathrm{r}} = 0.35$.[14] For the green-emitting Ir(ppy)$_3$ we take $\Gamma_{\mathrm{r}} = 0.816\ \mu\mathrm{s}^{-1}$ and $\Gamma_{\mathrm{nr}} = 0.249\ \mu\mathrm{s}^{-1}$,[15] leading to a radiative decay probability $\eta_{\mathrm{r}} = 0.77$, which agrees with the value $\eta_{\mathrm{r}} = 0.76$ given in Ref. 16. For the red-emitting Ir(MDQ)$_2$(acac) we take $\Gamma_{\mathrm{r}} = 0.588\ \mu\mathrm{s}^{-1}$ and $\Gamma_{\mathrm{nr}} = 0.112\ \mu\mathrm{s}^{-1}$ as obtained from $\eta_{\mathrm{r}} = 0.84$.[16,17] A typical value of $R_{\mathrm{F,diff}} = 1.5$ nm is taken for transfer in between green or red emitter molecules,[13] leading to exciton diffusion within the green- or red-emitting layer, while for the transfer from a green to a red emitter we take $R_{\mathrm{F,diff}} = R_{\mathrm{F,GR}} = 3.5$ nm, according to the estimate in Ref. 18. Transfer from red to green emitters should play no role and is therefore neglected.

No sufficiently detailed knowledge is as yet available about the molecular-scale mechanisms of TTA and TPQ. We investigate two possible scenarios, already explored by us in monochrome OLEDs and organic host-guest systems:[8,10,19] (1) immediate quenching of one triplet exciton when two triplet excitons or a triplet exciton and a charge appear on nearest-neighboring sites (short-range quenching); (2) quenching by Förster transfer of a triplet exciton to a site where another triplet exciton or a charge resides (long-range quenching). In the latter scenario the question is what to take for the Förster radii $R_{\mathrm{F,TPQ}}$ and $R_{\mathrm{F,TTA}}$. The simplest choice is $R_{\mathrm{F,TPQ}} = R_{\mathrm{F,TTA}} = R_{\mathrm{F,diff}}$, but this ignores the difference in the absorption spectrum of a molecule hosting a triplet exciton or a charge and the molecule in the ground state. Since further exciting an already excited molecule is much easier than exciting the molecule in the ground state, $R_{\mathrm{F,TPQ}}$ and $R_{\mathrm{F,TTA}}$ will be enhanced with respect to $R_{\mathrm{F,diff}}$. We will study the effect of equal enhancements of $R_{\mathrm{F,TPQ}}$ and $R_{\mathrm{F,TTA}}$ on the IQE.

We checked that without taking into account exciton quenching the simulated emission profile at a bias voltage

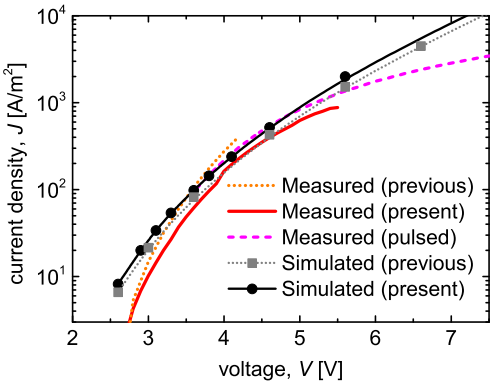

Figure 2. Previous[9] and present measurements as well as simulations of the current density-voltage characteristics, with results from pulsed measurements added. The errors in the simulated data are smaller than the displayed symbols.

$V = 3.6$ V is within the error bars equal to that displayed in Figure 2(b) of Ref. 9. The simulated current density-voltage, $J(V)$, characteristic is plotted in Figure 2, together with the characteristic of the non-integrated simulation approach from Ref. 9. Also these are essentially the same. Figure 2 also shows a remeasured $J(V)$ characteristic, together with the original measurement from Ref. 9. At high voltage the current density has decreased somewhat, pointing at a possible slight degradation. In addition, $J(V)$ data of a pulsed approach are given, which allows reaching higher voltages and current densities than with a dc approach, because the effects of heating are suppressed. The pulsed measurements were performed in three voltage regions with a duty cycle of 1% and with different pulse durations: for $V < 4$ V pulses of 1 s were used, for 4 V $< V <$ 6 V pulses of 0.1 s and for $V > 6$ V pulses of 50 μs. Since all data connect smoothly, we can conclude that relaxation effects due to the use of pulses are small. In a broad voltage range there is a good agreement between simulated and experimental results. The disagreement at high voltage (> 6 V) might be due to the use of Miller-Abrahams instead of Marcus hopping rates. The discrepancy at low voltage could be due to an underestimation of the trapping of holes by Ir(MDQ)$_2$(acac) in the red emitting layer.[9] The $J(V)$ characteristic of the simulations in which exciton quenching is included is indistinguishable from the one without exciton quenching (not displayed). From this we can conclude that exciton quenching has no significant influence on the current density.

Simulated results for the IQE are plotted as a function of J in Figure 3 and compared to the experimental IQE. The experimental IQE was obtained by dividing the luminescence as measured by a photodiode perpendicular to the OLED pixel by J and scaling the result such that at a bias of 3.6 V the IQE is 25%, corresponding to the measured external quantum efficiency (EQE) of 5%, using an integrating sphere, and the light-outcoupling efficiency of 20%.[9] The overall uncertainty in the IQE is estimated to be $\pm 5\%$. In the high current

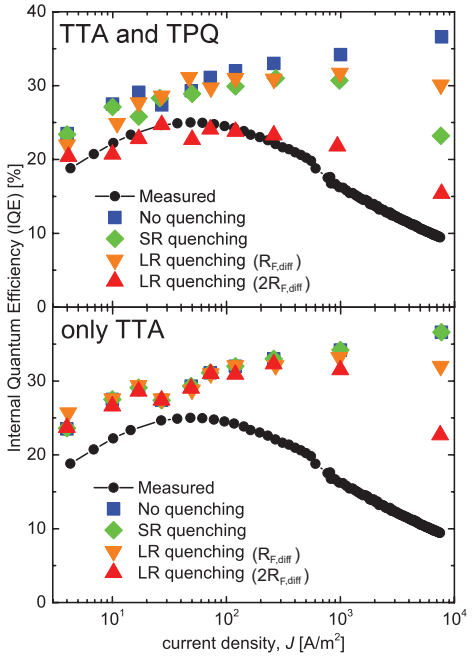

Figure 3. Measured and simulated internal quantum efficiency as a function of current density. The measured results have an overall uncertainty of $\pm 5\%$. Top: simulated results without quenching, with short-range (SR) nearest-neighbor quenching by triplet-triplet annihilation (TTA) and triplet-polaron quenching (TPQ), and with long-range (LR) quenching by TTA and TPQ with Förster quenching radii of 1.5 nm and 3 nm. The errors in the simulated data are of the order of the symbol size. Bottom: the same, but without TPQ.

density region $J > 500$ A/m^2, the IQE was obtained using the pulsed measurements. Only a small discontinuity is observed at the transition. The simulated results plotted in Figure 3 correspond to no quenching, short-range nearest-neighbor quenching, long-range quenching with $R_{\mathrm{F,TPQ}} = R_{\mathrm{F,TTA}} = R_{\mathrm{F,diff}}$, and long-range quenching with $R_{\mathrm{F,TPQ}} = R_{\mathrm{F,TTA}} = 2R_{\mathrm{F,diff}}$. The latter results, corresponding to $R_{\mathrm{F,TPQ}} = R_{\mathrm{F,TTA}} = 3$ nm for Ir(ppy)$_3$ and Ir(MDQ)$_2$(acac) and $R_{\mathrm{F,TPQ}} = R_{\mathrm{F,TTA}} = 7$ nm for quenching involving exciton transfer from Ir(ppy)$_3$ to Ir(MDQ)$_2$(acac), provide a fair description of the whole experimental IQE-J curve.

Satisfyingly, also the roll-on in the IQE at low J, i.e. the initial increase of the IQE with J, is properly described by the simulations. This roll-on occurs because with increasing current the fraction of excitons generated in the interlayer between the green- and blue-emitting layers, which are assumed to be lost, decreases. In the case of long-range quenching with a Förster radius of $2R_{\mathrm{F,diff}}$, there is in the low-J region also some effect of exciton quenching, bringing the simulated data right on top of the experimental data. The value of $R_{\mathrm{F,TTA}} = 2R_{\mathrm{F,diff}} = 3$ nm for both Ir(ppy)$_3$ and Ir(MDQ)$_2$(acac) is comparable to the reported values of 3.1 and 2.7 nm in thin films,[20] and 2.9 and 3.6 nm in solution,[21] for Ir(ppy)$_3$ and PtOEP, respectively.

To investigate the relative contributions of TTA and TPQ to exciton quenching, we plot in Figure 3 (bot-

tom) also the results of a simulation without TPQ. It is clear from these results that TTA is in our case only relevant for $J > 10^3$ A/m^2, which is far beyond the current density at which this OLED is typically operated (up to $J = 10^2$ A/m^2). Hence, the main cause for roll-off in the present OLED appears to be TPQ. This conclusion is in line with the conclusion drawn in Ref. 10 from simulations of prototypical phosphorescent green and red OLEDs based on Ir(ppy)$_3$ and PtOEP, respectively.

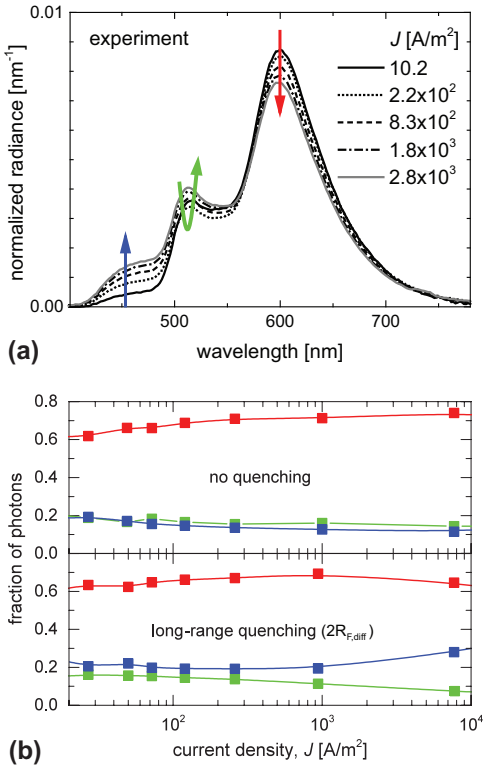

Figure 4. (a) Normalized measured spectra at different current densities J. The arrows indicate the trends in the relative contributions of the primary colors with increasing J. (b) Simulated results for the generated fractions of blue, green, and red photons without quenching (upper panel) and with long-range quenching by TTA and TPQ with a Förster radius of $2R_{\mathrm{F,diff}}$ (lower panel). The error in the simulated results is of the order of the symbol size.

To study whether also the change in color balance can be described by our modeling we display in Figure 4(a) the normalized spectra of the OLED at different current densities, measured with a Photo Research® SpectraScan® PR-705 spectrometer perpendicular to the OLED pixel, and in Figure 4(b) the fractions of the number of photons created in the red-, green-, and blue-emitting layers according to the simulations for the scenarios without quenching and with a Förster quenching radius of $2R_{\mathrm{F,diff}}$. Figure 4(b) shows that in agreement with our assumption that mainly triplet excitons suffer from quenching, the measured relative contribution of fluorescent blue emission increases with J at the expense of the phosphorescent red and green emission. The specific dependencies on J of the measured relative contributions of red emission (a monotonic decrease) and green emission (a decrease followed by an increase) in Figure 4(a) are not accurately reproduced by the simulations. Fine-tuning of the various involved Förster radii could improve the agreement. However, this would go beyond the present study, since then also various other refinements in the modeling should be considered. For example, part of the increase of the relative contribution of blue fluorescent emission with J may be due to singlet excitons produced by TTA (delayed fluorescence[22]) of the thus far disregarded triplet excitons in this layer.

This work was supported by the Dutch nanotechnology program NanoNextNL.

REFERENCES

[1] M. A. Baldo, D. F. O'Brien, Y. You, A. Shoustikov, S. Sibley, M. E. Thompson, and S. R. Forrest, Nature **395**, 151 (1998).
[2] C. Adachi, M. A. Baldo, M. E. Thompson, and S. R. Forrest, J. Appl. Phys. **90**, 5048 (2001).
[3] Y. Kawamura, K. Goushi, J. Brooks, J. J. Brown, H. Sasabe, and C. Adachi, Appl. Phys. Lett. **86** (2005).
[4] M. A. Baldo, C. Adachi, and S. R. Forrest, Phys. Rev. B **62**, 10967 (2000).
[5] J. Kalinowski, W. Stampor, J. Mężyk, M. Cocchi, D. Virgili, V. Fattori, and P. Di Marco, Phys. Rev. B **66**, 235321 (2002).
[6] S. Reineke, K. Walzer, and K. Leo, Phys. Rev. B **75**, 125328 (2007).
[7] N. C. Giebink, B. W. D'Andrade, M. S. Weaver, P. B. Mackenzie, J. J. Brown, M. E. Thompson, and S. R. Forrest, Journal of Applied Physics **103**, 044509 (2008).
[8] R. Coehoorn, H. van Eersel, P. A. Bobbert, and R. A. J. Janssen, Adv. Func. Mater. **25**, 2024 (2015).
[9] M. Mesta, M. Carvelli, R. J. de Vries, H. van Eersel, J. J. M. van der Holst, M. Schober, M. Furno, B. Lüssem, K. Leo, P. Loebl, R. Coehoorn, and P. A. Bobbert, Nature Mater. **12**, 652 (2013).
[10] H. van Eersel, P. A. Bobbert, R. A. J. Janssen, and R. Coehoorn, Appl. Phys. Lett. **105**, 143303 (2014).
[11] J. Cottaar, L. J. A. Koster, R. Coehoorn, and P. A. Bobbert, Phys. Rev. Lett. **107**, 136601 (2011).
[12] H. Yoshida and K. Yoshizaki, Org. Electron. **20**, 24 (2015).
[13] Y. Kawamura, J. Brooks, J. J. Brown, H. Sasabe, and C. Adachi, Phys. Rev. Lett. **96**, 017404 (2006).
[14] G. Li, C. H. Kim, Z. Zhou, J. Shinar, K. Okumoto, and Y. Shirota, Applied Physics Letters **88**, 253505 (2006).
[15] S. Mladenovski, S. Reineke, and K. Neyts, Opt. Lett. **34**, 1375 (2009).
[16] M. Furno, R. Meerheim, S. Hofmann, B. Lüssem, and K. Leo, Phys. Rev. B **85**, 115205 (2012).
[17] K.-C. Tang, K. L. Liu, and I.-C. Chen, Chem. Phys. Lett. **386**, 437 (2004).
[18] F. S. Steinbacher, R. Krause, A. Hunze, and A. Winnacker, Phys. Stat. Sol. A **209**, 340 (2012).
[19] H. van Eersel, P. A. Bobbert, and R. Coehoorn, J. Appl. Phys. **117**, 115502 (2015).
[20] Y. Zhang and S. R. Forrest, Chem. Phys. Lett. **590**, 106 (2013).
[21] W. Staroske, M. Pfeiffer, K. Leo, and M. Hoffmann, Phys. Rev. Lett. **98**, 197402 (2007).
[22] D. Y. Kondakov, T. D. Pawlik, T. K. Hatwar, and J. P. Spindler, J. Appl. Phys. **106**, 124510 (2009).